A 1024 × 8, 700-ps Time-Gated SPAD Line Sensor for Planetary Surface Exploration With Laser Raman Spectroscopy and LIBS

Yuki Maruyama, *Member, IEEE*, Jordana Blacksberg, and Edoardo Charbon, *Senior Member, IEEE*

***Abstract*—A 1024 × 8 time-gated, single-photon avalanche diode line sensor is presented for time-resolved laser Raman spectroscopy and laser-induced breakdown spectroscopy. Two different chip geometries were implemented and characterized. A type-I sensor has a maximum photon detection efficiency of 0.3% and median dark count rate of 80 Hz at 3 V of excess bias. A type-II sensor offers a maximum photon detection efficiency of 19.3% and a median dark count rate of 5.7 kHz at 3 V of excess bias. Both chips have 250-ps temporal resolution and fast gating capability, with a minimum gate width of 1.8 ns for type I and 0.7 ns for type II. Raman spectra were successfully observed from natural minerals, such as calcite and willemite. With the use of subnanosecond gating, background fluorescence was significantly reduced.**

***Index Terms*—Laser-induced breakdown spectroscopy (LIBS), Raman spectroscopy, single-photon avalanche diode (SPAD), single-photon counting, time gating.**

I. Introduction

SINGLE-PHOTON avalanche diode (SPAD) technology offers compact, highly sensitive photodetectors with subnanosecond temporal resolution [1]. In recent times, SPADs have also become available in standard complementary metal–oxide semiconductor (CMOS) technology [2]–[9], which allows for integration of high-performance circuitry such as on-chip time-to-digital converters and massively parallel data treatment [8], [9]. SPAD technology is already impacting various fields, such as positron emission tomography [6], range imaging [7], and Raman spectroscopy [11]. Raman spectroscopy is a nondestructive, label-free optical analysis technique used to obtain structural and compositional information without any advance sample preparation. For these reasons, *in situ* Raman spectrometers are proposed for many future planetary surface missions, for example, the ExoMars rover [12]. However, the Raman signature is often overwhelmed by strong fluorescence background in traditional continuous wave (CW) laser Raman spectroscopy. Due to its generation mechanism, the fluorescence background can be filtered out "in time domain" even though it overlaps the Raman signature in wavelength. To realize such functionality, highly sensitive time-resolved imagers, such as gated intensified charge-coupled devices (iCCDs) or streak cameras have been the sensors of choice. However, a solid-state sensor with similar performance would be preferable for space flight and planetary landings since solid-state sensors provide lower power consumption, lower operation voltage, smaller size, and higher durability. Solid-state streak cameras have emerged in the last few years to detect and image nanosecond-long optical phenomena [10]. A solid-state streak camera provides subnanosecond temporal resolution and a compact sensor, however, a greater number of photons is generally required due to the lack of intrinsic gain in standard photodiodes. Therefore, solid-state streak cameras are suitable to detect brighter phenomena, such as fluorescence lifetime but they have not yet been developed for time-resolved Raman spectroscopy.

Recently, time-gated SPAD image sensors have been proposed as a robust, solid-state alternative to streak cameras and gated iCCDs, due to their picosecond temporal resolution and single-photon detection capabilities. While image sensors based on SPADs have been studied in the past for time-resolved imaging modalities, such as fluorescence lifetime imaging microscopy [13], they have recently been proposed to tackle fluorescence background reduction from highly fluorescent minerals for laser Raman spectroscopy, targeting potential future on-surface planetary instruments [11]. However, due to long gating ($\sim$ 30 ns), the obtained Raman signature was contaminated by background noise, which limited detection of some weaker Raman peaks. In addition, due to extensive on-pixel electronics, the fill factor was reduced, resulting in low photon detection efficiency (PDE). To address both sensitivity and noise concerns, a larger SPAD with subnanosecond time-gating has been proposed and implemented as a single pixel, operated with a mechanical scanning stage to obtain a Raman signature [14]. The main limitation of this approach was the lack of simultaneous photon detection after dispersion, thus making the Raman detection a very long and possibly inaccurate process, due to the need for a much larger number of samples.

Manuscript received April 23, 2013; revised July 06, 2013; accepted August 12, 2013. Date of publication October 03, 2013; date of current version December 20, 2013. This paper was approved by Guest Editor Tadahiro Kuroda. Part of this work was carried out at the Jet Propulsion Laboratory, California Institute of Technology, under a contract with the National Aeronautics and Space Administration (NASA).

Y. Maruyama is with the Delft University of Technology, 2628 CD Delft, The Netherlands, and also with the Jet Propulsion Laboratory, California Institute of Technology, Pasadena, CA 91109 USA (e-mail: Yuki.Maruyama@jpl.nasa.gov).

J. Blacksberg is with the Jet Propulsion Laboratory, California Institute of Technology, Pasadena, CA 91109 USA.

E. Charbon is with the Delft University of Technology, 2628 CD Delft, The Netherlands.

Color versions of one or more of the figures in this paper are available online at http://ieeexplore.ieee.org.

Digital Object Identifier 10.1109/JSSC.2013.2282091

In addition, gated SPADs are valuable for laser-induced breakdown spectroscopy (LIBS) since the detector provides time information as well as intensity. LIBS is a rapid chemical analysis technique to measure elemental composition of the sample. High temperature micro-plasma is generated at the sample surface by a short laser pulse. Atomic emission lines can be observed when the plasma is cooled down. Since the optical setup of LIBS is similar to that of time-resolved Raman spectroscopy, gated SPADs can be used for these two fundamentally different spectroscopic techniques to add significant value to the instruments.

In this paper, this issue was addressed, while eliminating the need for any mechanically moving parts or multiple detectors to obtain a complete Raman signature. The paper presents two different types of line sensors each comprising an array of 1024×8 gated SPADs designed for time-resolved laser Raman spectroscopy and LIBS. The line sensors feature a minimum gate of 700 ps and a skew under 100 ps over the entire array.

This paper is organized as follows. Section II outlines the chip architecture and its implementation. Section III describes chip characterization. Section IV describes results from Raman spectroscopy and LIBS measurements, while Section V concludes the paper.

II. Chip Architecture

A. Gated SPAD Operation

A SPAD is a photodiode reverse biased above its breakdown voltage $V_{\rm bd}$, where the detector's optical gain is virtually infinite. To prevent permanent damage to the pn junction or wiring, a resistance is commonly used to passively quench the avalanche. Therefore, the SPAD creates a short voltage pulse per avalanche event and runs in a time-uncorrelated manner. In this work, three switches are implemented to achieve time-resolved photon detection, as shown in Fig. 1. The SPAD anode voltage can be modulated from V_{DD} to *GND* by alternately switching "Spadoff" and "Recharge." Therefore, the net voltage applied to the pn junction can be set V_e above breakdown voltage $V_{\rm bd}$ resulting in an optical gain change from 1 to infinity, as illustrated in Fig. 2. When a photon hits the multiplication region at the pn junction during the ON state, it creates an avalanche breakdown and the avalanche current charges up the anode capacitance $C_{\rm anode}$ to $V_{\rm bd}$. The avalanche breakdown is eventually quenched. This voltage change is captured by subsequently opened "Gate" switch, as shown in Fig. 3. When the photon hits the multiplication region during an OFF state, it will not trigger an avalanche but generates just a small current that can be ignored by the system. To bring the pixel from an OFF to an ON state, it is necessary to recharge the device, i.e., to bring the pn junction from $V_{\rm bd}$ to $V_{\rm bd} + V_e$, thus entering again into a Geiger mode of operation. This operation is completed through the "Recharge" transistor.

B. Chip Block Diagram

The block diagram of the system is shown in Fig. 4. The sensor consists of 16 groups of 64×8 SPAD arrays with fast readout interface electronics. Therefore, the chip has 8192 SPADs, or micro silicon photomultipliers (SiPMs), which need to be activated and deactivated precisely to achieve sub-nanosecond temporal resolution. The gate timing with respect to the laser pulse is controlled by a combination of off chip and on-chip delay lines. After the delay module, the trigger signal is copied into four control signals with slight temporal shift. Then, these control signals are propagated though properly balanced binary trees in order to minimize the skew between gating signals. Finally, short control pulses are generated by pulse generators based on the temporal difference of the control signals. Based on this architecture, two types of sensors are realized on the same die.

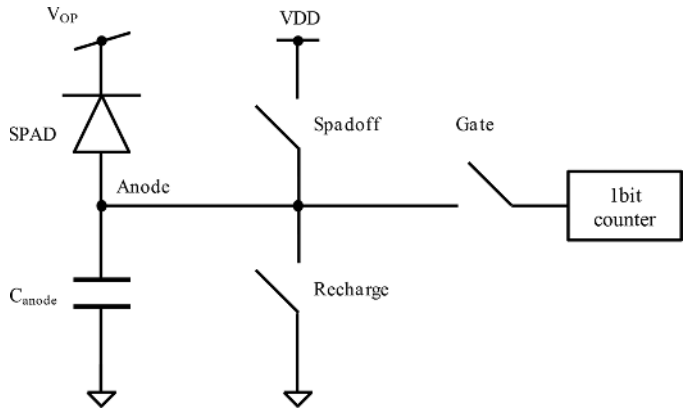

Fig. 1. Conceptual view of a gated SPAD.

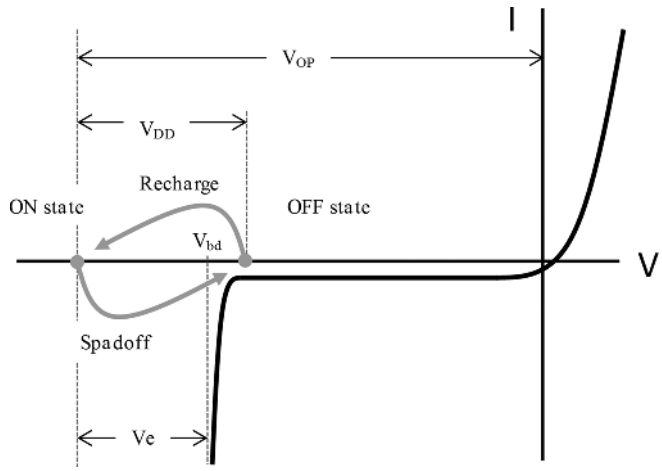

Fig. 2. Gating operation principle based on an active recharge technique.

C. Type I: Circular SPAD With All NMOS Control Circuits

Fig. 5(a) shows a schematic diagram of the type I architecture which consists of a circular SPAD, a NMOS 1-bit counter, a gating circuitry, as well as a readout interface circuit. This pixel structure is basically a shrunken-down version of the first chip used to demonstrate time-resolved Raman spectroscopy [11]. Since all control electronics are implemented in each pixel, this architecture is suitable for 2-D imaging applications such as fluorescence lifetime imaging microscopy (FLIM).

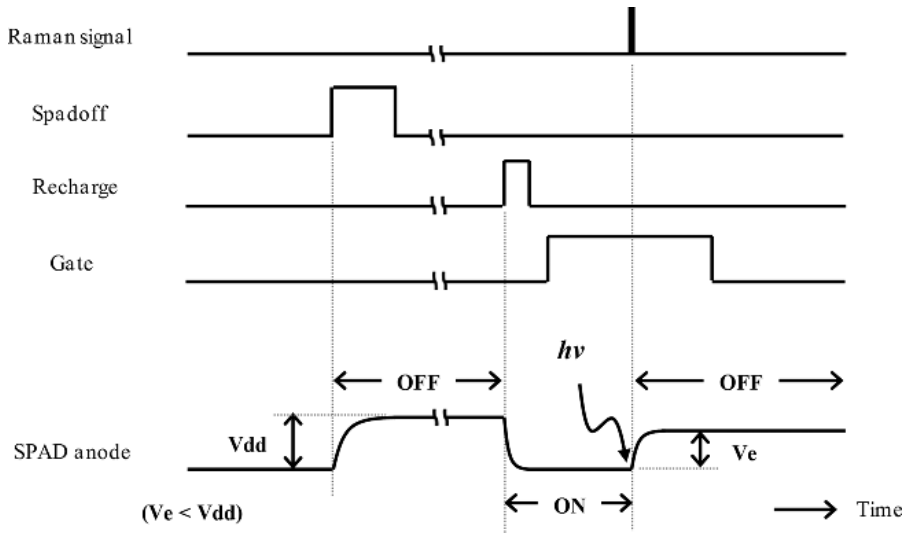

Fig. 3. Timing diagram of the gated operation.

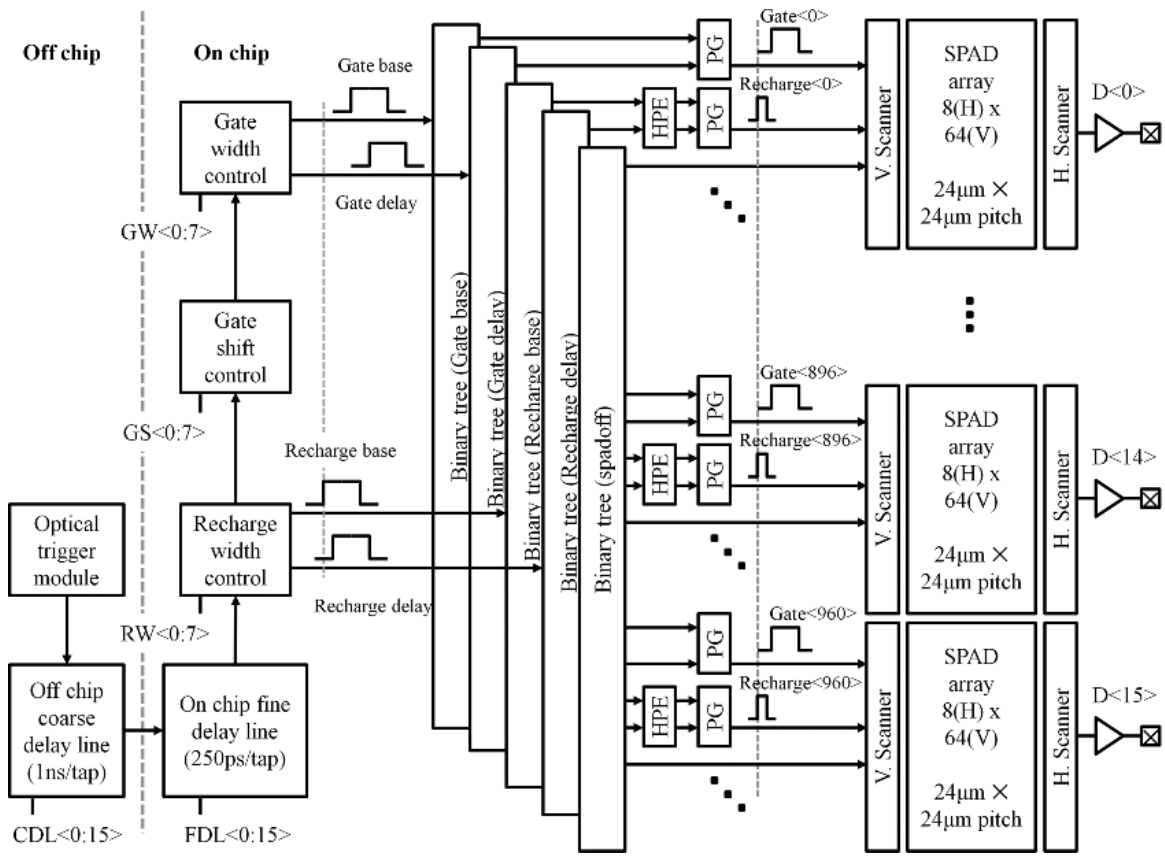

Fig. 4. System block diagram showing an optical trigger module, pulse width control units, off-chip and on-chip delay lines, binary trees, hot pixel elimination circuits (HPEs), pulse generators (PGs), and 16 groups of SPAD array.

D. Type II: Large Square-Shaped SPAD With In-Line Control Electronics

To improve PDE, large square-shaped SPADs with increased active area were designed. We report their full characterization in this paper. Each pixel comprises a large square-shaped SPAD, implemented as a shared cathode p+/deep n-well junction, a CMOS 1-bit counter, and a readout interface circuit as shown in Fig. 5(b). The type-II pixel is also equipped with an additional 1-bit memory hot pixel elimination module (HPE) to locally turn off noisy pixels. Each pixel can be operated both in time-correlated single-photon counting (TCSPC) and time-uncorrelated photon counting (TUPC) modes. Time-resolved laser Raman spectroscopy and LIBS are achieved through signals "spadoff" and "recharge," with a subsequently applied "gate" signal. These timing critical signals are propagated through binary trees and generated

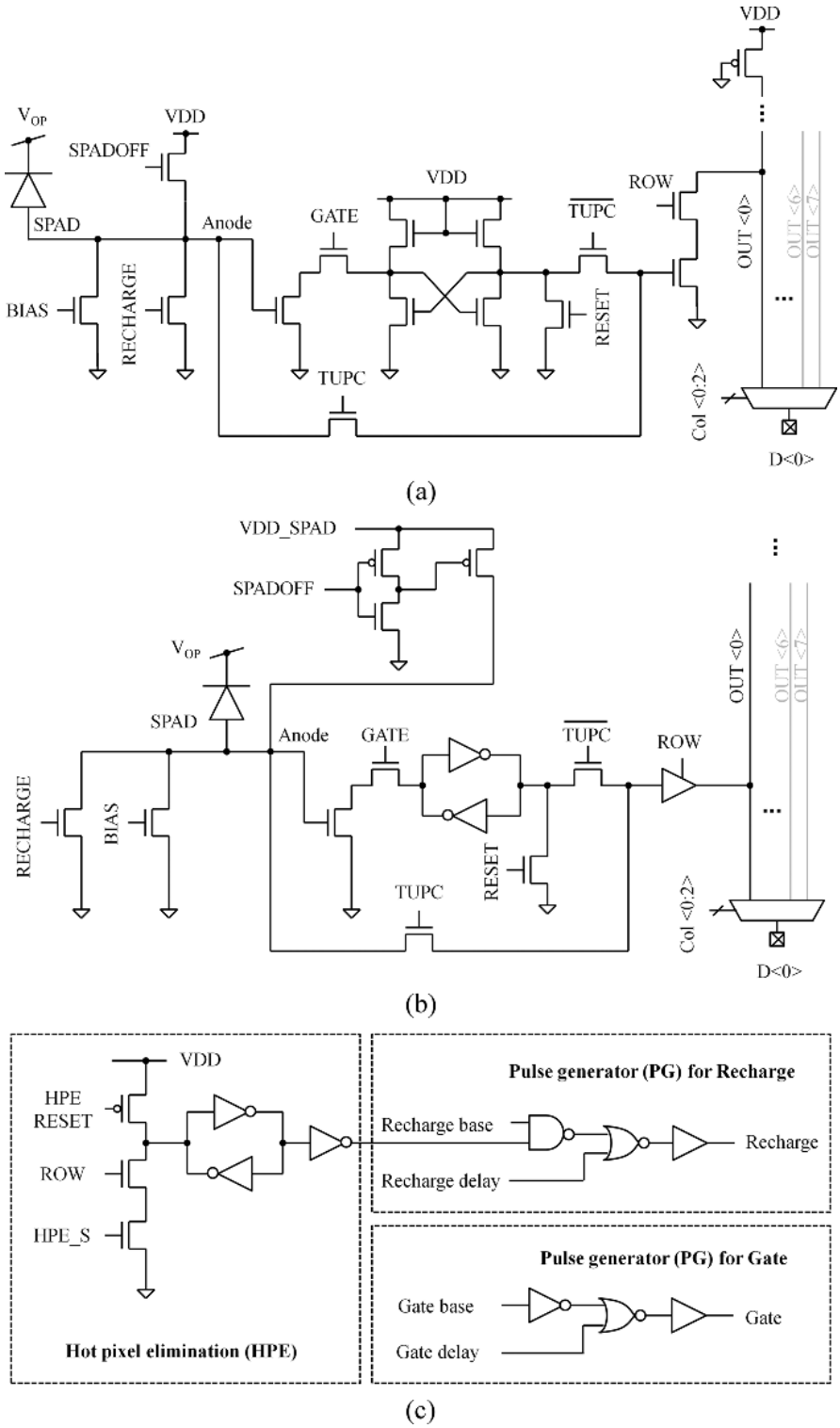

Fig. 5. Schematic of the time-resolved SPAD line sensors. (a) Type I: An all-NMOS pixel configuration. (b) Type II: A CMOS 1-bit counter with independent power line (V_{DD_SPAD}). (c) HPE module and PGs for the recharge and gate control signals.

by PGs in each, row as shown in Fig. 5(c). This architecture requires additional silicon real estate due to the need for two independent binary trees for each signal. However, this architecture was chosen to minimize the propagation length of the final short control pulses, recharge and gate, in order to minimize the impact of the dispersion on pulse width. In addition, thick metal layer was used to avoid skew variation caused by V_{DD} IR-drop. Decoupling capacitances were placed evenly across the entire binary tree to minimize dynamic V_{DD} variations. In addition, the type II pixel has an independent power line, V_{DD_SPAD}, which is separated from core V_{DD} (3.3 V). This additional feature allows increasing the excess bias V_e above 3.3 V by setting the V_{DD_SPAD} to 5 V.

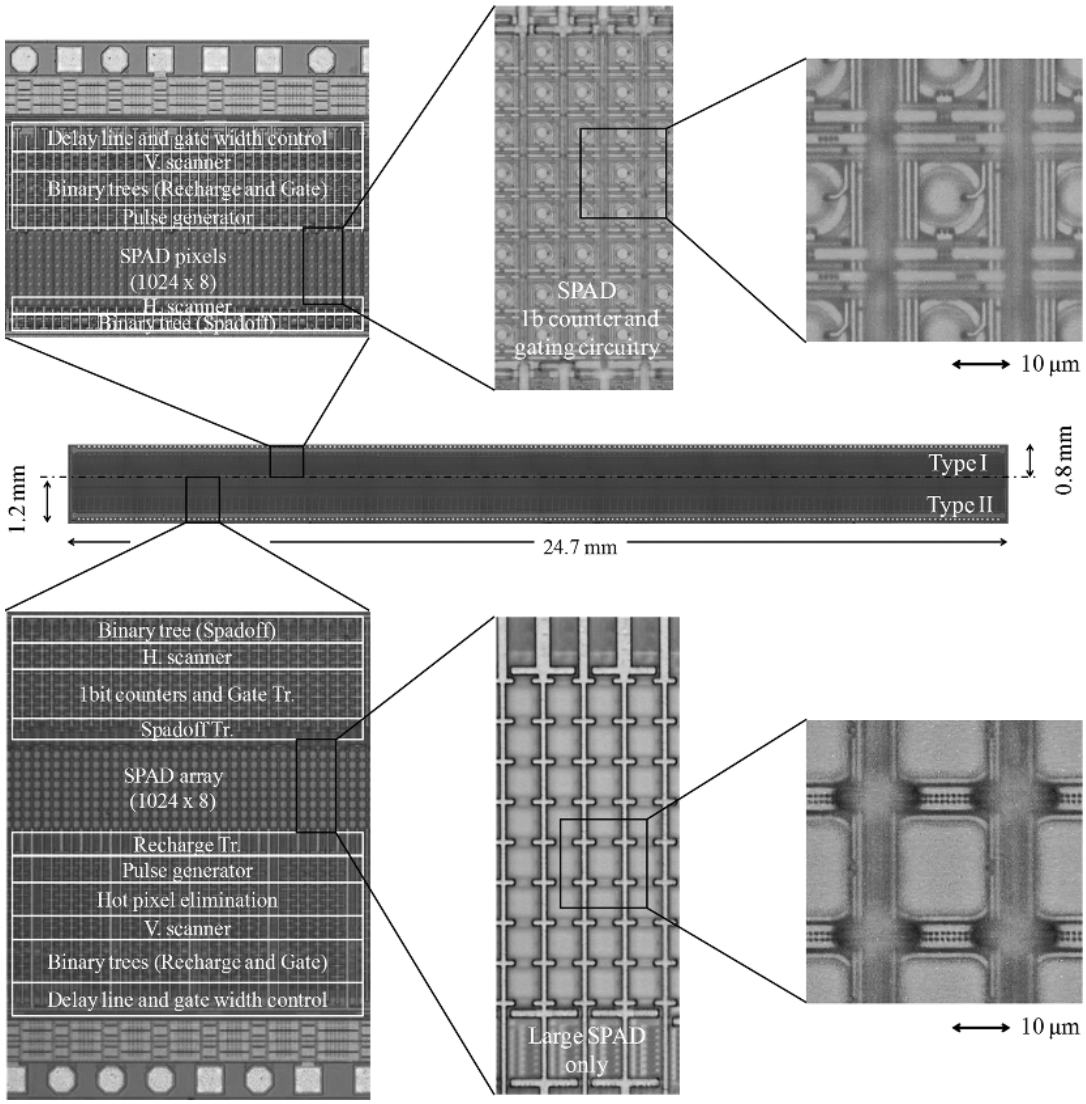

Fig. 6. Micrograph of the chip with a close-up. The chip consists of two versions of time-gated SPAD line sensors, denominated Type I and Type II. The chip was fabricated in standard 0.35-μm high-voltage CMOS technology.

E. Chip Realization

Fig. 6 shows the chip micrograph as well as a close-up of both sensors. The chip, fabricated in a 0.35 μm CMOS HV technology, has a total area of 49.4 mm^2 (Type I: 19.8 mm^2, Type II: 29.6 mm^2). A bonded chip as well as complete SPAD line sensor setup is shown in Fig. 7. The 24.6-mm-long focal plane matches the format of a typical detector that would be used at the output of a Raman spectrometer (e.g., CCD), allowing the observation of the entire Raman spectrum without the use of any moving parts. All necessary supply voltages are generated by the power module from 25-V input supply voltage. A Xilinx Spartan-3 FPGA and custom made C++ software was used to control the chip.

III. Characterization

A. Temporal Resolution

The SPAD gate width and its delay are controlled by a combination of off-chip (Maxim DS1020, 1 ns/tap) and on-chip delay lines (250 ps/tap) resulting in a temporal resolution of 250 ps through typical scan ranges of 32 ns. The differential nonlinearity (DNL) and integral nonlinearity (INL) of the delay lines are evaluated by measuring the gate signal output from the test pixel which is implemented in the farthest position from the trigger input in order to observe the worst case scenario. The DNL and INL were measured in a range of $\pm$ 0.27 LSB and $\pm$0.89 LSB, respectively, with a bin width of 250 ps. The results are shown in Fig. 8.

B. Gating Width

The gating performance was characterized in terms of its width and skew variations across the entire 24.7-mm-long chip. A 405-nm pulsed laser source (Advanced Laser Diode Systems, Germany) with FWHM pulse width of 34 ps was used to trigger an avalanche at the same time across the entire array. By scanning the gate window with respect to the laser pulse, the gate width and skew variation can be extracted as illustrated in Fig. 9.

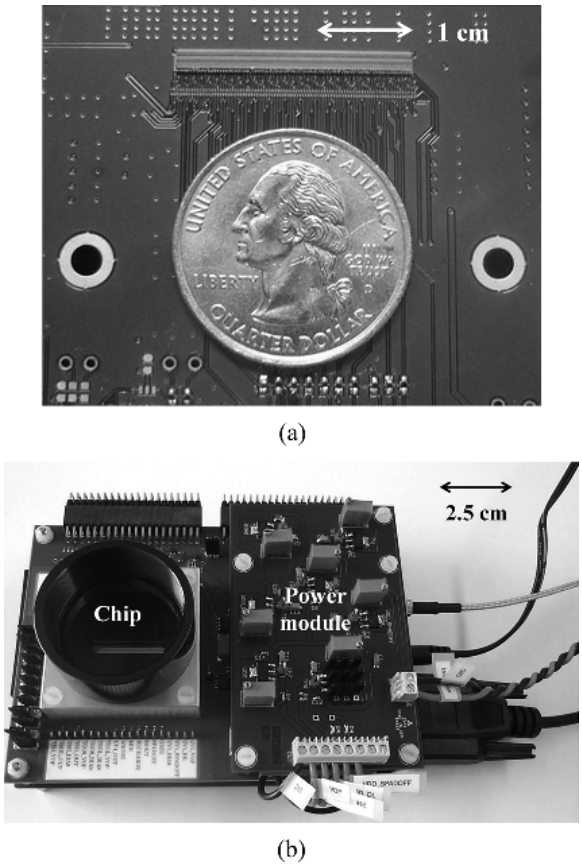

Fig. 7. (a) Photograph of the line sensor mounted as chip-on-board. (b) Complete SPAD line sensor setup.

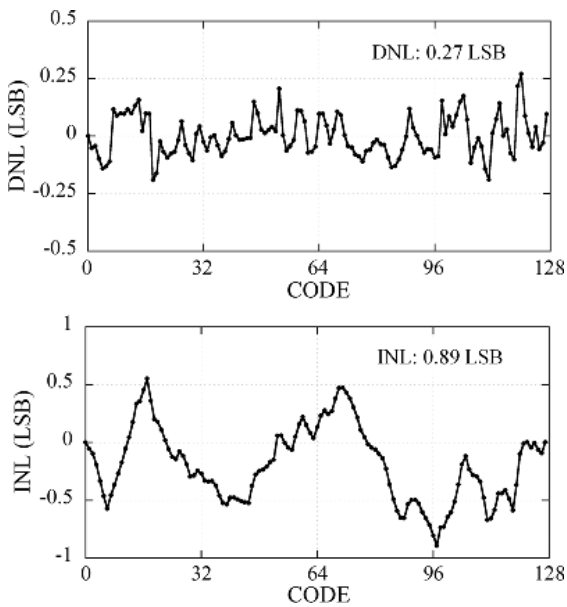

Fig. 8. Measured DNL and INL of the combined on-chip/off chip delay lines at room temperature. Code 128 represents a delay of 32 ns.

Fig. 10(a) shows three examples of different gate widths verified optically. The horizontal axis represents time and the vertical axis is pixel position. The results shown here are measured using the type-II sensor. The figure shows that the pixels are activated and deactivated with an accuracy better than 250 ps and a negligible skew. The optimal gate width for operation is chosen from 0.7 to 12.6 ns based on the photon return from the sample and the excitation laser pulse width. Fig. 10(b) summarizes the FWHM gate width variation for various gate widths. The optically measured minimum gate width is 0.7 ns ($\sigma = 120$ ps).

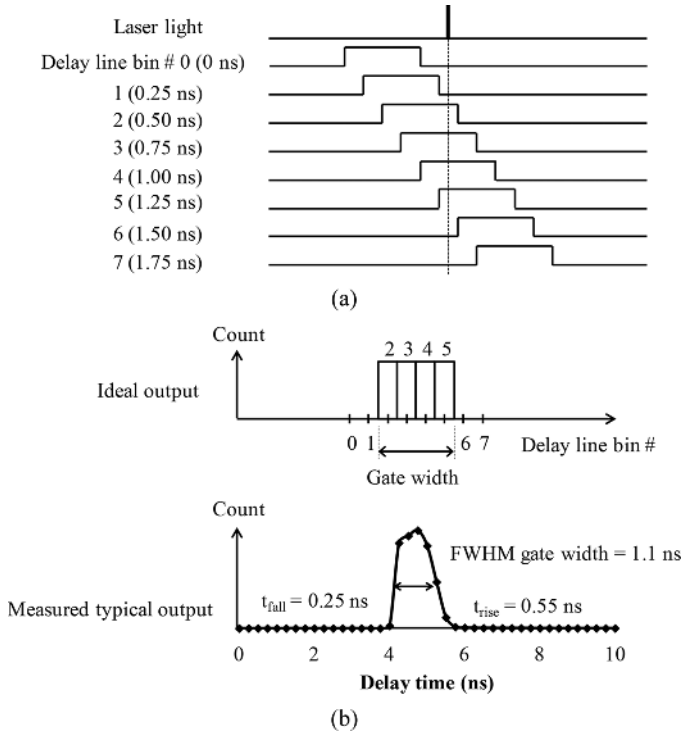

Fig. 9. (a) Gate-width measurement scheme. (b) Measured 1.1-ns gate width with rise and fall time.

C. Photon Detection Efficiency (PDE)

Fig. 11 plots the PDE, defined as the detected photon number divided by the incident photon number in a normalized time interval. The PDE was measured at various excess biases V_e under uniform lighting with a 465-nm light-emitting device (LED). The PDE of the type-I and type-II chips are 0.3% and 10.2% at V_e of 3 V, respectively. The SPAD implemented in this work includes p-implanted guard rings to prevent premature edge breakdown and maintain uniform breakdown across the entire p+ active area. The implantation-based guard ring tends to become larger than that of drawn size due to thermal annealing during the fabrication process. Thus, the actual SPAD has an inactive distance from the p+/p- guard ring boundary, which is experimentally estimated as 1.75 μm for these devices. Therefore, the type-II sensor has 32 times higher sensitivity compared with that of the type-I sensor, even though the drawn p+ active area difference is only 9.1 times. Detailed analysis of the inactive distance can be found in an earlier study [15]. The median dark count rate (DCR) of these devices is 80 Hz and 5.7 kHz at an excess bias of 3 V, respectively. A benefit of gated operation is that the probability of detecting a dark count is decreased by the gate ON/OFF ratio. For example, the probability of the dark count of the type-II sensor is as low as $4 \times 10^{-4}\%$ at the minimum gate width of 0.7 ns. Therefore, DCR is not a problem when using sub-nanosecond gating.

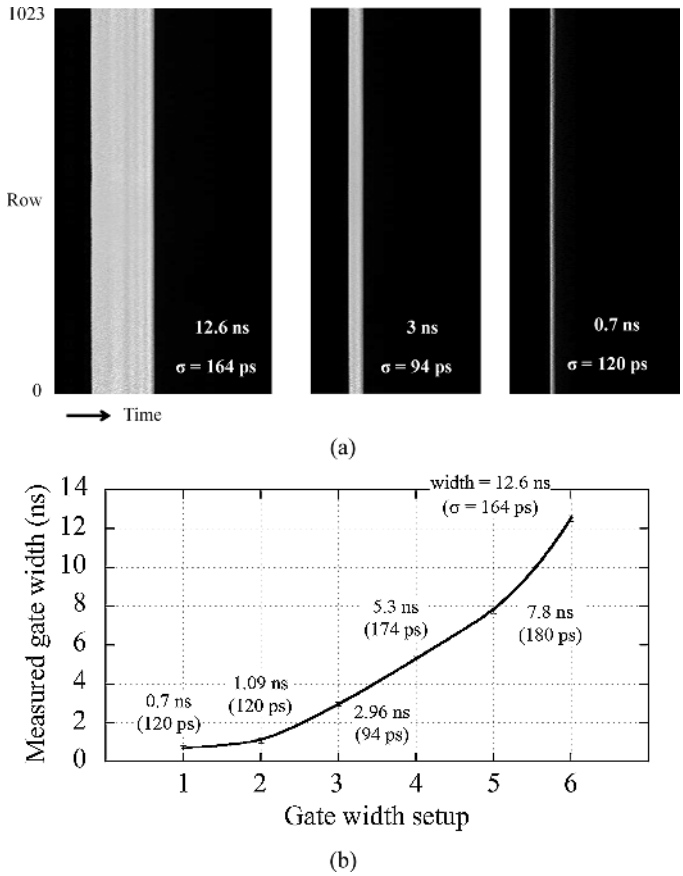

Fig. 10. Optically measured gate width from the Type-II sensor. (a) Output images at 12.6-, 3-, and 0.7-ns gate width. (b) Summary of the gate width.

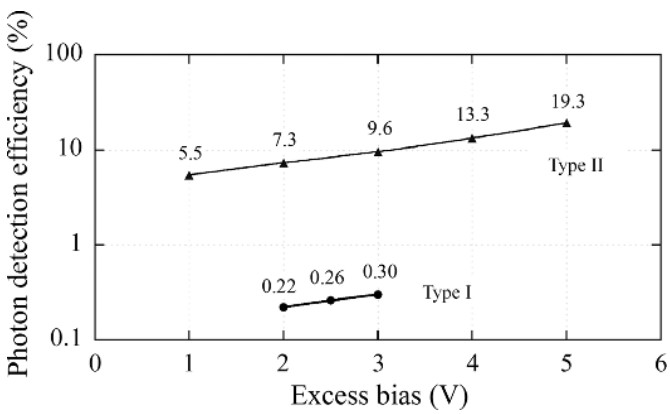

Fig. 11. Comparison of the PDE between the type-I and type-II sensors measured at 465 nm. The exact values of the PDE are shown on the plot.

In addition, due to the separated V_{DD_SPAD}, the type-II chip can be operated at even higher V_e, resulting in a significantly higher PDE of 19.3% at V_e of 5 V with a slightly higher DCR of 43 kHz.

D. Hot Pixel Elimination (HPE)

One concern in the SPAD array was hot pixels, which generate very high dark counts and create optical crosstalk to neighboring pixels due to photoemission caused by impact ionization. An additional static random access memory (SRAM) was implemented to disable noisy pixels, as shown in Fig. 5(c). While

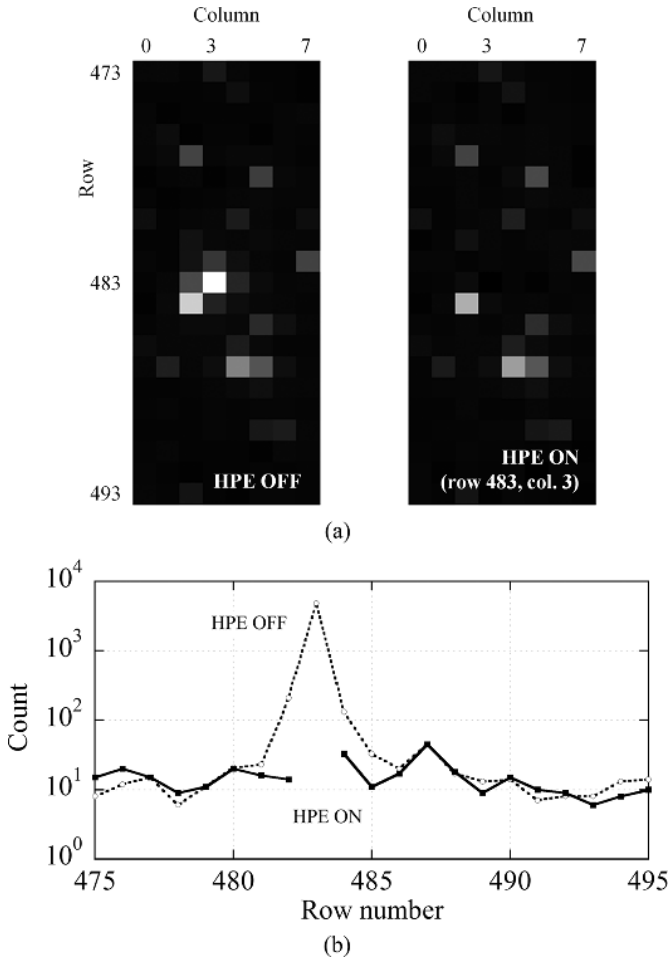

Fig. 12. HPE performance measured in the dark at excess bias of 4 V with gate width of 16 ns. (a) A section of the array with a hot pixel present and after hot pixel elimination. (b) DCR distribution around a hot pixel. The activity of surrounding pixels caused by photon emission from hot pixels is reduced significantly.

HPE_RSET is off, the writing procedure to the HPE module is enabled by Row signal and HPE_S. When the data of the SRAM is high, the recharge pulse is disabled and the SPAD is never turned on until the next HPE_RESET is applied. Fig. 12 clearly shows an array with a noisy pixel at its center before and after the pixel is permanently turned off by the hot pixel elimination (HPE) module. This is a simple technique to remove noisy pixels, and it is essential wherever noisy pixels become problematic at higher excess bias conditions [16].

IV. Time-Resolved Raman Spectroscopy and LIBS

Fig. 13 shows the optical setup of the laser Raman spectrometer. The time-resolved Raman/LIBS spectrometer was originally equipped with a streak camera [17]. Replacing the streak camera with a SPAD line sensor allows for lower power dissipation, and lighter weight with reduced complexity. The Raman signature generated at the sample was projected onto the chip through a spectrometer. A 532 nm ($\sim$ 20 μJ/pulse, $\sim$ 400-ps pulse width, TEEM Photonics) 1-kHz pulsed laser, with neutral density filters to reduce the power on the sample, was used to create the Raman signature. Since the laser repetition rate is 1 kHz, the sensor has 1 ms of relaxation time

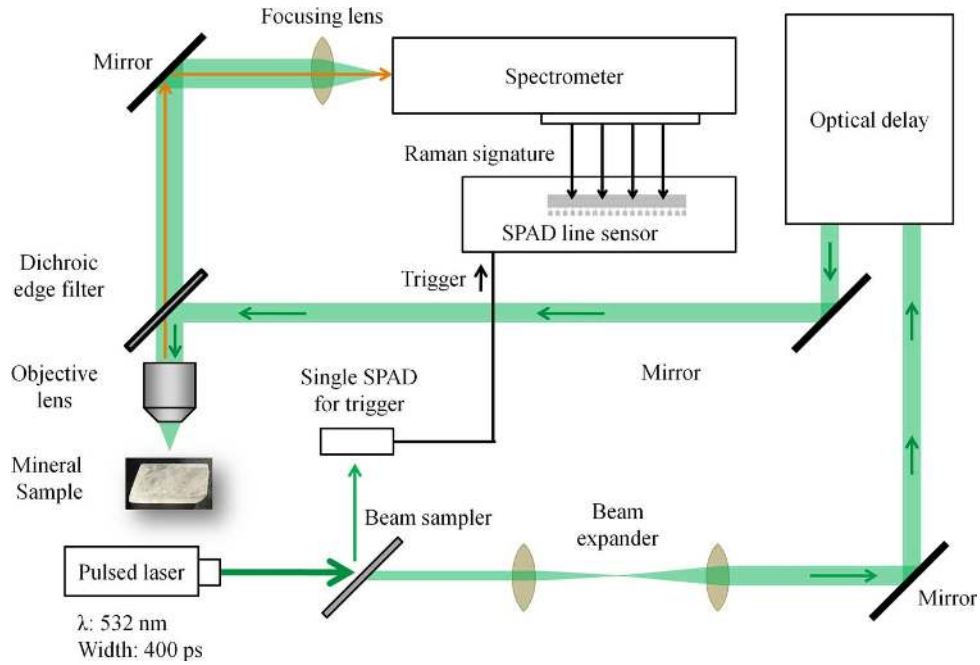

Fig. 13. Optical setup of the laser Raman/LIBS combined spectrometer.

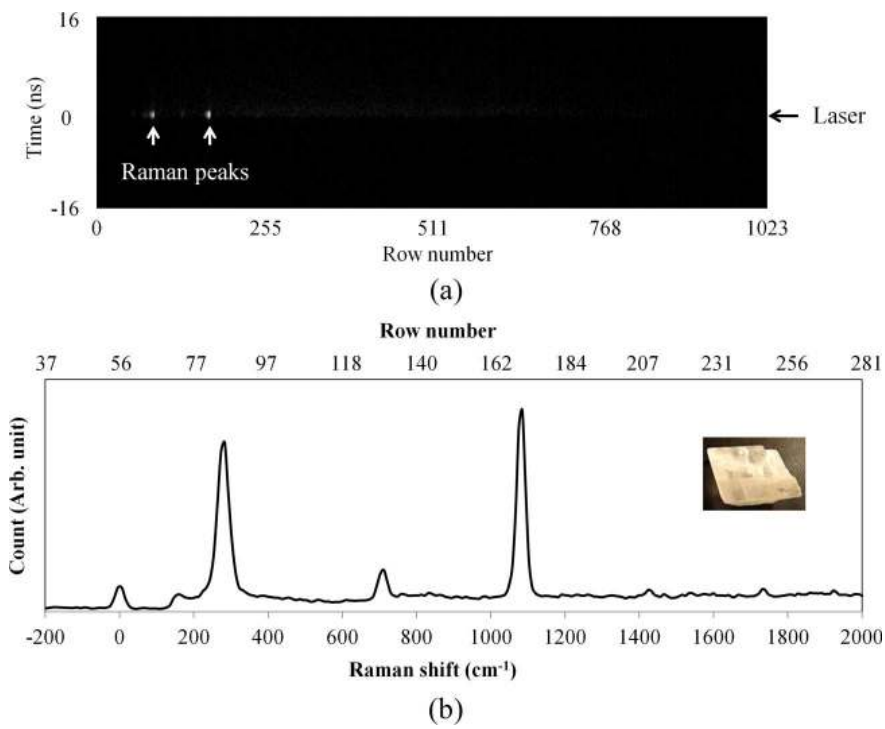

Fig. 14. (a) Calcite Raman signature measure in time. (b) Calcite Raman peaks observed at laser excitation period with 3-ns gate width integrated over 10 k gating cycles.

to release trapped carriers created by the previous avalanche. In other words, there is no effective afterpulsing from the previous gating period since afterpulsing occurs in the first few microseconds from the prior avalanche event. A tiny fraction of the laser light was used as an optical trigger to synchronize the detector and the pulsed laser. A single pixel SPAD based trigger module was used to convert the optical trigger pulses to electrical trigger signals. The gating window shift with respect to the laser pulse allows us to obtain the Raman signature distribution in time with 250-ps temporal resolution. In this study, the type-II sensor was chosen as a detector for the experiments shown hereafter since the type-II sensor has significantly higher sensitivity than that of the type-I sensor. However, both sensors can be used for time-resolved Raman spectroscopy and LIBS. Fig. 14(a) shows the Raman signature obtained from calcite with 3 ns gating width in each delay line bin of 250 ps. The output of 8 columns was summed in each row at each delay time. Fig. 14(b) shows Raman peaks

TABLE I
PERFORMANCE SUMMARY OF THE TIME-RESOLVED SPAD LINE SENSORS

	Type I	Type II	Unit
Array format	1024 × 8		
Chip size	24.7 × 0.8	24.7 × 1.2	mm
Pixel pitch	24		μm
SPAD breakdown voltage	20.4	19.6	V
Fill factor (calculated from p+/nwell junction area)	4.9	44.3	%
Dark count rate	80 (V_e = 3 V)	5.7 k (V_e = 3 V), 43 k (V_e = 5 V)	Hz
Minimum gate width (FWHM)	1.75 (V_e = 3 V)	0.7 (V_e = 3 V)	ns
Dark count probability per gating at min. gate width	1.4×10^{-5}	4.0×10^{-4}	%
Photon detection efficiency (PDE) at 465 nm	0.3 (V_e = 3 V)	9.6 (V_e = 3 V), 19.3 (V_e = 5 V)	%
Gating rep. rate	1 to 950		cycle/sec
Vdd voltage	3.3		V
Current dissipation (Vdd)	81	0.4	mA
Delay range	0 to 32 (typical)		ns
Temporal resolution	250		ps
Delay line DNL (0 to 32ns)	68 (0.27 LSB)		ps
Delay line INL (0 to 32ns)	223 (0.89 LSB)		ps

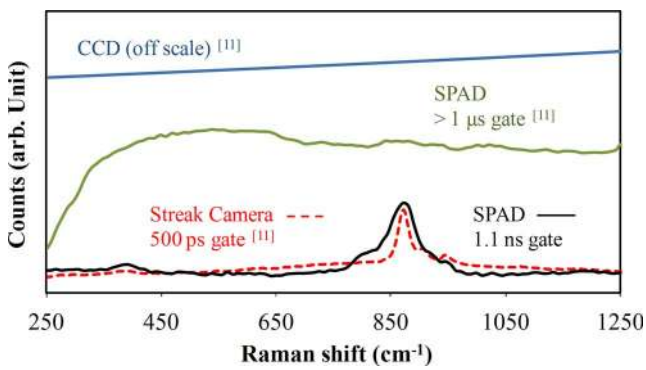

Fig. 15. Willemite Raman signature measure with 1.1-ns gate integrated over 64 k gating cycles.

measured at time zero where laser pulses were hitting the sample. The Raman spectra were successfully observed with high signal-to-noise ratio without any cooling, commonly used in CCD based CW Raman spectrometers under development for *in situ* planetary exploration [18], [19]. To demonstrate fluorescence rejection capability with nanosecond gating, a natural mineral willemite was chosen as a sample, since willemite has a strong fluorescence background in the wavelength region of interest for Raman spectroscopy. Fig. 15 shows the Raman spectrum observed from willemite. The figure also shows a comparison of the results obtained in this work with a continuously operated CCD camera, a streak camera, and a SPAD imager with $> \mu$s-long gating window.

The sensor was subsequently used to demonstrate its potential in a combined Raman/LIBS instrument for planetary science applications. Fig. 16(a) shows an artist's rendering of the Curiosity rover analyzing the elemental composition of a rock on Mars using its laser-induced remote sensing instrument (ChemCam). The proposed SPAD line sensor is intended for use in a similar manner targeting not only LIBS but also time-resolved Raman spectroscopy [20]. Preliminary

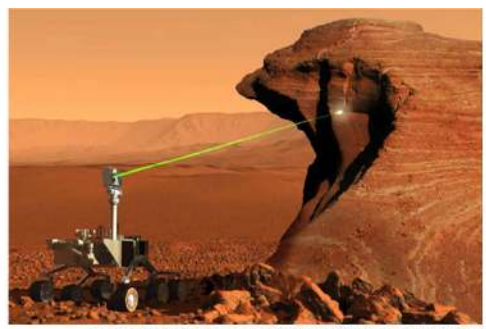

(a)

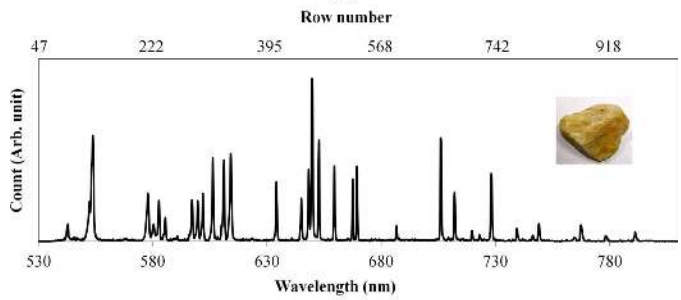

(b)

Fig. 16. (a) Artist's rendering of the LIBS instrument (ChemCam) on the Curiosity rover analyzing a rock on the surface of Mars. (b) LIBS spectrum from barite at 120 ns after the laser pulse.

LIBS results show barium atomic emission lines from barite at 120 ns after the laser pulse as shown in Fig. 16(b). In the case of LIBS, a broadband laser-induced plasma appears prior to the atomic emission lines. Therefore, properly applying the delay with respect to the laser pulse allows for removal of the plasma background. The LIBS lines can be used to determine elemental composition of rock and soil samples. Table I summarizes the performance of the chip, whereas Table II shows a comparison table with state-of-the-art sensors.

TABLE II
COMPARISON WITH OTHER STATE-OF-THE-ART GATED SPAD IMAGERS

	This work		Pancheri et al. [13]	Blacksberg et al. [11]	Nissinen et al. [14]	Unit
	Type I	Type II				
Technology	CMOS 0.35μm HV		CMOS 0.35μm HV	CMOS 0.35μm HV	CMOS 0.35μm HV	
Array format	1024 × 8		64 × 1	128 × 128	1	
Focal plane length	24,576		1,664	3,200	20	μm
Detector pitch	24		26	25	N/A	μm
Fill factor (calculated from p+/nwell junction area)	4.9	44.3	34	4.5	11	%
PDP	34 (λ = 465nm, Ve = 3 V)		32 (λ = 450 nm, Ve = 3.3V)	N/A	N/A	%
PDE	0.3 (V_e = 3 V)	9.6 (V_e = 3 V) 19.3 (V_e = 5 V)	N/A	5 (V_e = 5 V, w/ microlens)		%
DCR	80 (median, V_e = 3 V)	5.7 k (median, V_e = 3 V)	1 k (typ., V_e = 3.3 V)	160 (median, V_e = 3.3 V)	11 k (typ., V_e = 3.3 V)	Hz
Min. gate window	1.75 (V_e – 3 V)	0.7 (V_e – 3 V)	0.8	7	0.3	ns
Dark count probability per gating	1.4×10^{-5} (V_e = 3 V)	4.0×10^{-4} (V_e = 3 V)	1.6×10^{-4}	1.1×10^{-4}	3.3×10^{-4}	%
Application	Raman and LIBS		FLIM	Raman	Raman	

V. CONCLUSION

This paper presented a new application field of SPADs where single-photon sensitivity and subnanosecond temporal resolution are required. Two different sensor architectures, Type I and Type II, were implemented in 0.35-μm high-voltage CMOS process and characterized in terms of noise, sensitivity, as well as temporal resolution. Finally, the Raman signature from highly fluorescent mineral samples was successfully observed, which was impossible to obtain in CW laser Raman spectroscopy with 532-nm excitation. These signals are in good agreement with the results obtained with a streak camera, which requires high voltage and greater complexity with larger volume and weight. This work shows a successful implementation of a single solid-state sensor for a combined Raman and LIBS instrument. Such an instrument would have wide application to planetary science where phase identification and elemental composition provide a deeper understanding of the history and evolution of diverse planetary surfaces.

REFERENCES

[1] S. Cova, A. Longoni, and A. Andreoni, "Towards picosecond resolution with single-photon avalanche diodes," *Rev. Sci. Instrum.*, vol. 52, pp. 408–412, Mar. 1981.

[2] J. C. Jackson, A. P. Morrison, P. Hurley, W. R. Harrell, D. Damjanovic, B. Lane, and A. Mathewson, "Process monitoring and defect characterization of single photon avalanche diodes," in *Proc. Int. Conf. Microelectron. Test Structures,* , vol. 14, pp. 165–170, Mar. 2001.

[3] A. Rochas, A. R. Pauchard, P. A. Besse, D. Pantec, Z. Prijic, and R. S. Popovic, "Low-noise silicon avalanche photodiodes fabricated in conventional CMOS technologies," *IEEE Trans. Electron Devices*, vol. 49, no. 3, pp. 387–394, Mar. 2002.

[4] J. A. Richardson, E. A. G. Webster, L. A. Grant, and R. K. Henderson, "Scalable single-photon avalanche diode structures in nanometer CMOS technology," *IEEE Trans. Electron Devices*, vol. 58, no. 7, pp. 2028–2035, Jul. 2011.

[5] S. Mandai, M. Fishburn, Y. Maruyama, and E. Charbon, "A wide spectral range single-photon avalanche diode fabricated in an advanced 180 nm CMOS technology," *Opt. Exp.*, vol. 20, pp. 5849–5857, Mar. 2012.

[6] L. H. Brage, L. Gasparini, L. Grant, R. K. Henderson, N. Massari, M. Perenzoni, D. Stoppa, and R. Waker, "An 8 × 16-pixel 92 kSPAD time-resolved sensor with on-pixel 64 ps 12 b TDC and 100 MS/s real-time energy histogramming in 0.13 μm CIS technology for PET/MRI Applications," in *IEEE Int. Solid-State Circuits Conf. Dig. Tech. Papers*, Jan. 2013, pp. 486–487.

[7] C. Niclass, M. Soga, H. Matsubara, M. Ogawa, and M. Kagami, "A 0.18 μm CMOS SoC for a 100 -range 10 ps 200 × 96-pixel time-of-flight depth sensor," in *IEEE Int. Solid-State Circuits Conf. Dig. Tech. Papers*, Jan. 2013, pp. 488–489.

[8] M. Gersbach, Y. Maruyama, R. Trimananda, M. W. Fishburn, D. Stoppa, J. A. Richardson, R. Walker, R. Henderson, and E. Charbon, "A time-resolved, low-noise single-photon image sensor fabricated in deep-submicron CMOS technology," *IEEE J. Solid-State Circuits*, vol. 47, no. 6, pp. 1394–1407, Jun. 2012.

[9] C. Veerappan, J. Richardson, R. Walker, D. U. Li, M. W. Fishburn, Y. Maruyama, D. Stoppa, F. Borghetti, M. Gersbach, R. K. Henderson, and E. Charbon, "A 160 × 128 single-photon image sensor with on-pixel 55 ps 10 bit time-to-digital converter," in *IEEE Int. Solid-State Circuits Conf. Dig. Tech. Papers*, Feb. 2011, pp. 312–314.

[10] M. Zlatansky and W. Uhring, "Streak-mode optical sensor in standard BiCMOS technology," *IEEE Proc. Sensors*, pp. 1604–1607, Oct. 2011.

[11] J. Blacksberg, Y. Maruyama, E. Charbon, and R. George, "Fast single-photon avalanche diode arrays for laser Raman spectroscopy," *Opt. Lett.*, vol. 36, pp. 3672–3674, Sep. 2011.

[12] J. A. Grant and F. Westall, "Two rovers to the same site on Mars, 2018: Possibilities for cooperative science," *Astrobiol.*, vol. 10, pp. 663–685, 2010.

[13] L. Pancheri *et al.*, "A SPAD-based pixel linear array for high-speed time-gated fluorescence lifetime imaging," in *Proc. IEEE ESSCIRC*, Sep. 2009, pp. 428–431.

[14] I. Nissinen, J. Nissinen, A. Lansman, L. Hallman, A. Kilpela, J. Kostamovaara, M. Kogler, M. Aikio, and J. Tenhunen, "A sub-ns time-gated CMOS single photon avalanche diode detector for Raman spectroscopy," in *Proc. IEEE ESSDERC*, Sep. 2011, pp. 375–378.

[15] M. W. Fishburn, Y. Maruyama, and E. Charbon, "Reduction of fixed-position noise in position-sensitive single-photon avalanche diodes," *IEEE Trans. Electron Devices*, vol. 58, no. 8, pp. 2354–2361, Aug. 2011.

[16] Y. Maruyama and E. Charbon, "A time-gated 128 × 128 CMOS SPAD array for on-chip fluorescence detection," in *Proc. Int. Image Sensor Workshop*, Jun. 2011, pp. 270–273.

[17] J. Blacksberg, G. R. Rossman, and A. Glecker, "Time-resolved Raman Spectroscopy for in situ planetary mineralogy," *Appl. Opt.*, vol. 49, pp. 4951–4962, Sep. 2010.

[18] R. Ingley, I. B. Hutchinson, H. G. M. Edwards, A. G. Moral, E. Diaz, G. Ramos, O. Barcos, C. P. Canora, F. Rull, C. Tato, and P. Pool, "ExoMars Raman laser spectrometer breadboard: Detector design and performance," in *Proc. SPIE*, Sep. 2011, vol. 8152, pp. 815215-1–815215-9.

[19] B. Ahlers, I. Hutchinson, and R. Ingley, "Combined Raman/LIBS spectrometer elegant breadboard – built and tested – and flight model spectrometer unit," in *Proc. Int. Conf. Space Opt.*, Oct. 2008.

[20] J. Blacksberg, Y. Maruyama, M. Choukroun, E. Charbon, and G. R. Rossman, "New microscopic laser-coupled spectroscopy instrument combining Raman, LIBS, and fluorescence for planetary surface mineralogy," in *Proc. 43rd Lunar and Planetary Sci. Conf.*, Mar. 2012, p. 1510.

Yuki Maruyama (M'13) received the B.E. and M.S. degrees in electrical and electronic engineering and Ph.D. degree in electrical and information engineering from Toyohashi University of Technology, Aichi, Japan, in 2003, 2005, and 2008, respectively.

He was a Doctoral Research Fellow (DC2) and a Postdoctoral Research Fellow (PD) of the Japan Society of Promotion of Science (JSPS), Tokyo, Japan in 2007 and 2008, respectively. He was a Postdoctoral Researcher with Delft University of Technology, Delft, The Netherlands, from 2009 to 2012. He is currently with the Jet Propulsion Laboratory, Pasadena, CA, USA, developing time-gated SPAD line sensors for time-resolved Raman spectroscopy.

Jordana Blacksberg received the B.S.E. degree from the University of Pennsylvania, Philadelphia, PA, USA, in 1994, and the M.S. and Ph.D. degrees from the University of California, Berkeley, CA, USA, in 1997 and 2001, respectively, all in materials science and engineering.

She has 12 years of experience in planetary instrument and detector development. She is the Principle Investigator on the time-resolved laser spectrometer for planetary Raman spectroscopy at the Jet Propulsion Laboratory, California Institute of Technology, Pasadena, CA, USA. She has also developed numerous detectors for imaging and spectroscopy in bands ranging from UV to far-IR including delta-doped CCDs, Germanium BIB arrays, and extended wavelength silicon detectors.

Edoardo Charbon (M'92–SM'11) received the Diploma from ETH Zurich, Zurich, Switzerland, in 1988, the M.S. degree from the University of California at San Diego, La Jolla, CA, USA, in 1991, and the Ph.D. degree from the University of California, Berkeley, CA, USA, in 1995, all in electrical engineering and computer science.

From 1995 to 2000, he was with Cadence Design Systems, where he was the architect of the company's intellectual property protection and information hiding projects; from 2000 to 2002, he was Canesta Inc.'s Chief Architect, leading the development of the company's 3D camera technology; Canesta was sold to Microsoft Corporation in 2010. Since 2002, he has been a member of the Faculty of EPFL and in 2008 he has become Chair of VLSI Design at the Delft University of Technology, Delft, The Netherlands, working on single-photon image sensors and quantum security devices. He is the initiator and coordinator of MEGAFRAME and SPADnet, two EC funded projects for CMOS photon counting image sensors to be used in biomedical diagnostics; he is a Principle Investigator in EndoTOFPET-US and PicoSec, two projects aimed at the design of endoscopic PET sensors. He has authored and coauthored over 250 articles in technical journals and conference proceedings and two books, and he holds 14 patents.

Dr. Charbon was the corecipient of 2012 European Photonics Innovation Award.